iScience

CellPress
OPEN ACCESS

Article

Somatic *Dnmt3a* inactivation leads to slow, canonical DNA methylation loss in murine hematopoietic cells

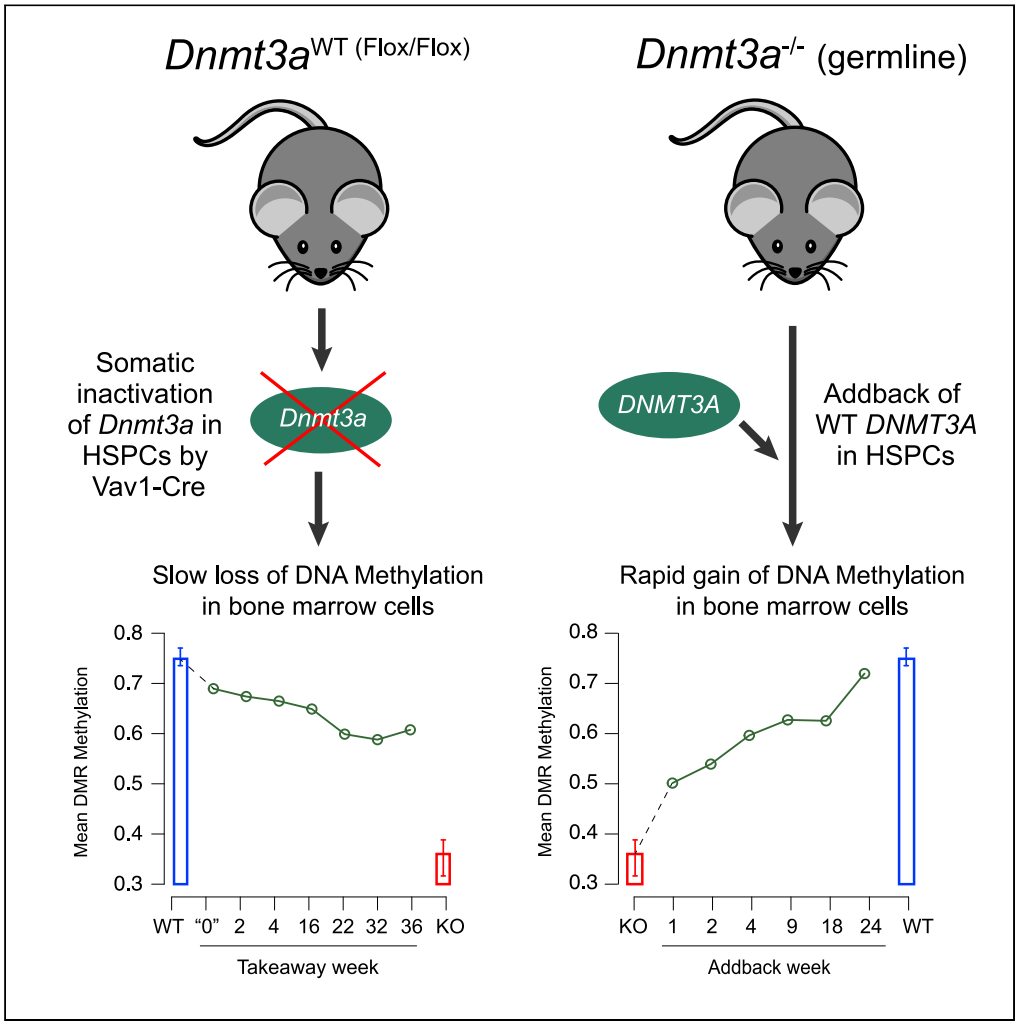

Amanda M. Smith, Angela M. Verdoni, Haley J. Abel, ..., Elizabeth R. Leight, Christopher A. Miller, Timothy J. Ley

timley@wustl.edu

Highlights

Somatic inactivation of *Dnmt3a* in hematopoietic cells causes slow DNA methylation loss

Methylation loss occurs in an ordered fashion, at canonical sites in the genome

Many genomic regions that lose or gain methylation rapidly are overlapping

Methylation remodeling is an integrated process involving methylases and demethylases

Smith et al., iScience 25, 104004
April 15, 2022
https://doi.org/10.1016/j.isci.2022.104004

iScience

CellPress
OPEN ACCESS

Article

Somatic *Dnmt3a* inactivation leads to slow, canonical DNA methylation loss in murine hematopoietic cells

Amanda M. Smith,[1,6] Angela M. Verdoni,[1,3,6] Haley J. Abel,[1] David Y. Chen,[2] Shamika Ketkar,[1,4] Elizabeth R. Leight,[1,5] Christopher A. Miller,[1] and Timothy J. Ley[1,7,*]

SUMMARY

Mutations in the gene encoding DNA methyltransferase 3A (*DNMT3A*) are the most common cause of clonal hematopoiesis and are among the most common initiating events of acute myeloid leukemia (AML). Studies in germline and somatic *Dnmt3a* knockout mice have identified focal, canonical hypomethylation phenotypes in hematopoietic cells; however, the kinetics of methylation loss following acquired *DNMT3A* inactivation in hematopoietic cells is essentially unknown. Therefore, we evaluated a somatic, inducible model of hematopoietic *Dnmt3a* loss, and show that inactivation of *Dnmt3a* in murine hematopoietic cells results in a relatively slow loss of methylation at canonical sites throughout the genome; in contrast, remethylation of Dnmt3a deficient genomes in hematopoietic cells occurs much more quickly. This data suggests that slow methylation loss may contribute, at least in part, to the long latent period that characterizes clonal expansion and leukemia development in individuals with acquired *DNMT3A* mutations in hematopoietic stem cells.

INTRODUCTION

The deposition and maintenance of methyl groups on mammalian DNA is mediated by DNA methyltransferases. Dysregulation and mutations of methyltransferase genes are well recognized contributors to the pathogenesis of many tumor types. For example, somatic mutations in *DNMT3A* are the most common cause of age-related clonal hematopoiesis (Xie et al., 2014; Jaiswal et al., 2014; Genovese et al., 2014). Furthermore, *DNMT3A* is mutated in approximately 20% of *de novo* acute myeloid leukemia (AML) and >30% of normal karyotype AML (Renneville et al., 2012; Marcucci et al., 2012) making it one of the most common AML initiating mutations. Over 60% of AML-associated *DNMT3A* mutations are heterozygous missense mutations at the codon for amino acid R882 (Ley et al., 2010; Gaidzik et al., 2013; Gale et al., 2015). Mechanistic studies have shown that the R882H mutation encodes a dominant negative protein that creates a methyltransferase "sink" that sequesters the WT protein into relatively inactive complexes. This inhibits formation of active homodimers, reducing its enzymatic activity by approximately 80% (Russler-Germain et al., 2014). Reduction of enzymatic activity leads to a focal, canonical hypomethylation phenotype both in non-leukemic blood cells (Smith et al., 2021) and in AML cells expressing the R882H mutation (Spencer et al., 2017). However, many aspects of this process are not yet understood, including the rate of methylation loss in HSPCs (and their progeny) over time. In this report, we show that somatic inactivation of *Dnmt3a* in the hematopoietic cells of adult mice results in a very slow loss of CpG methylation at predictable, canonical sites throughout the genome. These findings have implications for understanding the long latency and subtle phenotypes associated with *DNMT3A* mutations that cause clonal hematopoiesis and AML.

RESULTS

Kinetics of DNA methylation loss in mouse bone marrow cells after somatic Dnmt3a inactivation

To better understand the kinetics of methylation loss following inactivation of *Dnmt3a* (*Dnmt3a* 'takeaway'), we utilized an inducible Cre-ER^{TM} system to delete both endogenous *Dnmt3a* alleles in transplanted hematopoietic cells (annotated *Dnmt3a*$^{fl/fl}$ + Tam; wild-type controls annotated *Dnmt3a*$^{fl/fl}$ – Tam (WT);

[1]Division of Oncology, Section of Stem Cell Biology, Department of Internal Medicine, Washington University School of Medicine, St. Louis, MO 63110, USA

[2]Division of Dermatology, Department of Internal Medicine, Washington University School of Medicine, St. Louis, MO 63110, USA

[3]Present address: Vitalant, Pittsburgh, PA 15213, USA

[4]Present address: Department of Molecular and Human Genetics, Baylor College of Medicine, Houston, TX 77030, USA

[5]Present address: Leight Medical Communications, LLC, St. Charles, MO 63303, USA

[6]These authors contributed equally

[7]Lead contact

*Correspondence: timley@wustl.edu

https://doi.org/10.1016/j.isci.2022.104004

Figure 1A). Cre-mediated deletion of exon 19 (flanked by loxP sites) leads to out-of-frame splicing of the mRNAs encoding all active isoforms (Kaneda et al., 2004). To limit the deletion to hematopoietic cells, we used a secondary transplant model, which allowed us to ameliorate any deleterious effects of deleting *Dnmt3a* in non-hematopoietic tissues (Figure 1B). Importantly, floxing of *Dnmt3a* was not performed until we confirmed engraftment at 4-weeks posttransplant, to minimize the stress of transplantation as a potential confounding variable. Floxing efficiency in whole bone marrow (WBM) following tamoxifen dosing (9 doses administered over 3 weeks) was established with RT-PCR at the time of sacrifice and was compared to no-tamoxifen controls for each timepoint, when available. *Dnmt3a* floxing efficiency was >90% in nearly all tested mice, and was rapidly achieved, because it had occurred in approximately 90% of measured alleles at "week 1", which was four weeks after the first dose of tamoxifen was given (Figure 1C). Importantly, *Dnmt3a* deletion did not confer a disadvantage to the transplanted cells, because floxing efficiency was maintained above 90% until the end of the experiment, 36 weeks after the final dose of tamoxifen was given.

We defined differentially methylated regions (DMRs) from whole-genome bisulfite sequencing (WGBS) by comparing $Dnmt3a^{-/-}$ germline knockout bone marrow cells (from 6 independent mice), vs. non-floxed $Dnmt3a^{fl/fl}$ marrow (from 8 independent mice), which corresponded to *Dnmt3a* null and *Dnmt3a* wild-type levels, respectively. DMRs were required to have >10 CpGs, a mean methylation difference between the two groups of >0.2, a false discovery rate (FDR) of <0.05 and within-group standard deviations in methylation levels <0.1, parameters established in previous work (Ketkar et al., 2020). Contiguous DMRs within 50 base pairs (bp) of each other were merged. Using these criteria, we identified 33,519 DMRs in the $Dnmt3a^{-/-}$ samples; 33,503 (99.96%) of these were hypomethylated (Figure 1D). The genomic locations and annotations for all of these DMRs (and how they were affected by the takeaway and addback experiments at each time point) are shown in Table S1. Passively plotting the methylation values of the $Dnmt3a^{fl/fl}$ + Tam (takeaway) samples at these 33,519 DMRs revealed a progressive, time-dependent loss of methylation for some but not all regions, and the degree of methylation loss did not reach $Dnmt3a^{-/-}$ (knockout) levels even at the latest time points (Figures 1D and 1E). The methylation loss occurred in a canonical and ordered way, where hypomethylated DMRs in week 1 were also present in subsequent weeks; additional methylation loss progressed over time at the same sites, suggesting that DMR location or sequence context was deterministic for these patterns.

Characteristics of genomic regions that are sensitive or refractory to DNA methylation loss caused by Dnmt3a inactivation

Next, we defined DMRs occurring in the late takeaway samples by comparing the same set of WT samples to the pooled takeaway samples from weeks 22, 32, and 36, which had similar methylation patterns. Using the same criteria described above for calling DMRs, we identified a total of 1,605 DMRs with this analysis. Nearly all (1603/1605, 99.88%) were hypomethylated, as shown in the heat map of Figure 2A, and Table S2. Of these late takeaway DMRs, 1328 (83%) overlapped with the *Dnmt3a* null DMRs defined above. The mean methylation beta value of the 277 nonoverlapping DMRs was 0.38 $\pm$ 0.17 SD, significantly less than that of the mean beta value for WT bone marrow cells at the same regions (0.73 $\pm$ 0.14 SD, $p = 8.2 \times 10^{-155}$, 2-sided paired t-test). *Dnmt3a* KO samples were also hypomethylated in the same 277 regions (mean beta value 0.46 $\pm$ 0.19 SD, $p = 3.1 \times 10^{-97}$ compared to WT values), only slightly less so. Of these 277 DMRs, 273 were hypomethylated in both the late takeaway and Dnmt3a KO samples.

We also investigated the characteristics of the DMRs that were "refractory" to methylation loss in the late takeaway samples to determine whether they had unique features or genomic locations that altered their methylation fates. Late takeaway DMRs were classified based on the change in mean beta methylation values between the WT samples and the last 3 takeaway timepoints (from weeks 22, 32, 36). Late takeaway DMRs with an absolute mean beta value change of <0.1 were classified as 'unchanged' (i.e., refractory to methylation loss, n = 10,945); DMRs with absolute mean change >0.2 were concordant with the Dnmt3a KO samples (n = 8,240). The genomic annotations of these regions are shown in Figure 2B; the refractory regions were enriched for CpG islands (which have the lowest levels of methylation of all the annotated regions). Conversely, the regions that did become hypomethylated in the late takeaway samples were significantly enriched for shores, shelves, gene bodies, and promoters.

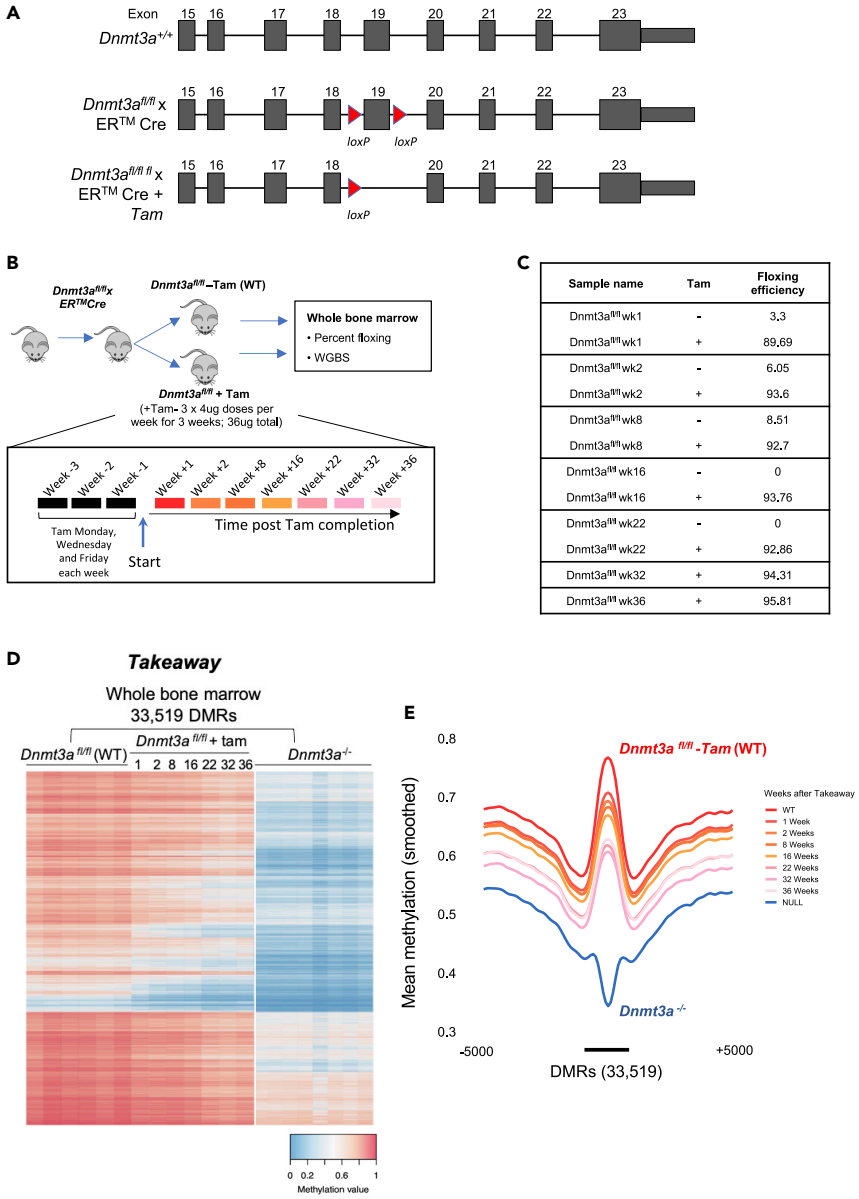

Figure 1. Methylation loss following *Dnmt3a* deletion is time dependent and slow

(A) Schematic representation of the knockout strategy. Exons are represented as filled boxes and loxP sites as red triangles. Tam, tamoxifen.

(B) Schematic representation of the *Dnmt3a* takeaway experiment. Tam, tamoxifen; WGBS, whole genome bisulfite sequencing.

(C) Table of floxing efficiencies determined by quantitative RT-PCR.

(D) Heatmap of mean methylation values for 33,519 DMRs identified by comparing $Dnmt3a^{fl/fl}$ – Tam (WT) vs. $Dnmt3a^{-/-}$ (without dox; null), with mean methylation values for Tam-treated takeaway samples plotted passively. Time of Tam (takeaway) treatment is shown in weeks.

(E) Methylation density of 33,519 DMRs defined in *d*, in $Dnmt3a^{fl/fl}$ + Tam. DMR; differentially methylated region, tam; tamoxifen, WGBS; whole genome bisulfite sequencing. Time is shown in weeks. Data are presented as means over all DMRs and all samples from each treatment group: $Dnmt3a^{-/-}$ (N = 8), $Dnmt3a^{fl/fl}$ + Tam (N = 6), N = 1 for each takeaway timepoint.

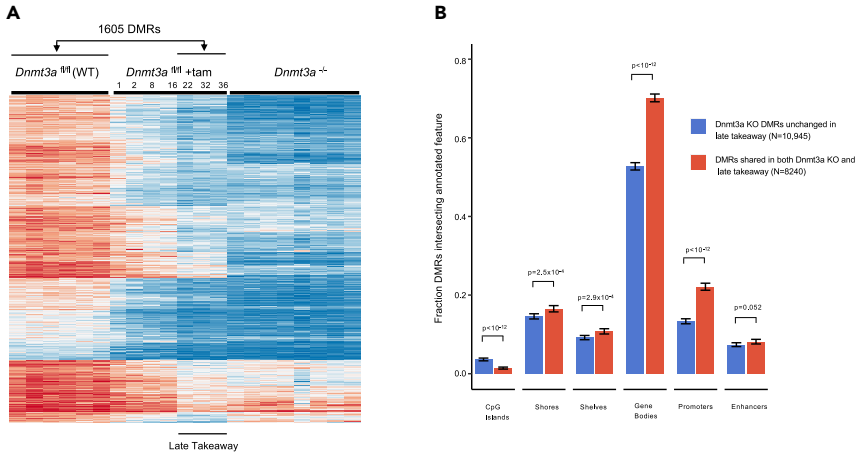

Figure 2. Comparison of WT vs *Dnmt3a* KO DMRs to Late Takeaway DMRs

(A) Heatmap of mean methylation values for 1605 DMRs identified by comparing WT bone marrow samples vs. the last 3 takeaway timepoints, i.e., *Dnmt3a*$^{fl/fl}$ + Tamoxifen at weeks 22, 32, 36 ("Late Takeaway"). Mean methylation values for the additional takeaway timepoints and *Dnmt3a*$^{-/-}$ (without dox; null) are plotted passively. Time after the completion of Tamoxifen treatment is shown in weeks.

(B) Enrichment of annotated features in subsets of Dnmt3a KO DMRs that also changed in the late takeaway samples, vs. those that did not change. DMRs were classified based on the change in mean methylation values between WT bone marrow samples, and the last 3 takeaway timepoints (weeks 22, 32, and 36). DMRs with an absolute mean beta value change of <0.1 were classified as non-changing ('refractory'); DMRs with absolute mean beta value change of >0.2 were classified as changing. 95% Wilson score confidence intervals and Fisher's exact p-values are shown.

Kinetics of remethylation in Dnmt3a deficient bone marrow cells with DNMT3A addback

Next, we utilized previously published data from our lab that measured the kinetics and patterns of remethylation in *Dnmt3a* null mice that contained an 'addback' Dox-inducible *DNMT3A* transgene (Figure 3A) (Ketkar et al., 2020). By comparing the fate of DMRs in the takeaway and addback experiments, we were able to assess whether the changes were concordant. Remethylation of most of the 33,519 DMRs occurred rapidly following expression of *DNMT3A* transgene in *Dnmt3a*$^{-/-}$ mice treated with Dox, so that methylation levels approached that of WT mice by 24 weeks. This suggests that methylation loss after *Dnmt3a* inactivation occurs much more slowly than remethylation of *Dnmt3a*-dependent sites after restoration of *DNMT3A* activity (Figures 3B and 3C). This trend was true across all functionally annotated regions of the genome, including CpG islands, gene bodies, promoters, and enhancers (Figure 3D). However, there was variation in the level of methylation in different annotated regions of the genome in wild-type bone marrow cells. For example, enhancer regions and gene bodies had higher levels of baseline methylation (red square) compared to promoters and CpG islands (i.e., there is a higher level of methylation in these regions, even in the absence of *Dnmt3a*; blue square). This suggests that some regions of the genome have additional, Dnmt3a-independent mechanisms for methylating and/or maintaining CpG methylation. Interestingly, the baseline methylation levels did not appear to dictate rates of methylation loss with takeaway (or methylation gain with addback) because these rates were consistent across all genomic regions assessed (Figure 3D). Further, promoter DMRs were significantly smaller in size, compared to DMRs in genes and enhancers (Figure 3E), and CpG islands had significantly higher CpG density per DMR compared to other annotated regions (Figure 3F), factors which may influence their levels of basal methylation.

Characteristics of dynamic DMRs

We next wanted to understand the characteristics of 'dynamic DMRs' — those DMRs that lose and gain methylation as a function of time — to determine whether these represent the same regions with takeaway and addback. We defined a dynamic DMR as one that moves >0.2 (i.e., a 20% change in methylation density) away from baseline at the assessed timepoint. For dynamic *takeaway* DMRs, the baseline was *Dnmt3a*$^{fl/fl}$ – Tam (WT) methylation levels; for dynamic *addback* DMRs, the baseline was *Dnmt3a*$^{-/-}$ methylation levels. As time progressed, additional dynamic DMRs were observed (Figure 4A). However, even at week 36 after takeaway, only ~1/3 of DMRs were dynamic. In contrast, nearly 100% of DMRs were dynamic

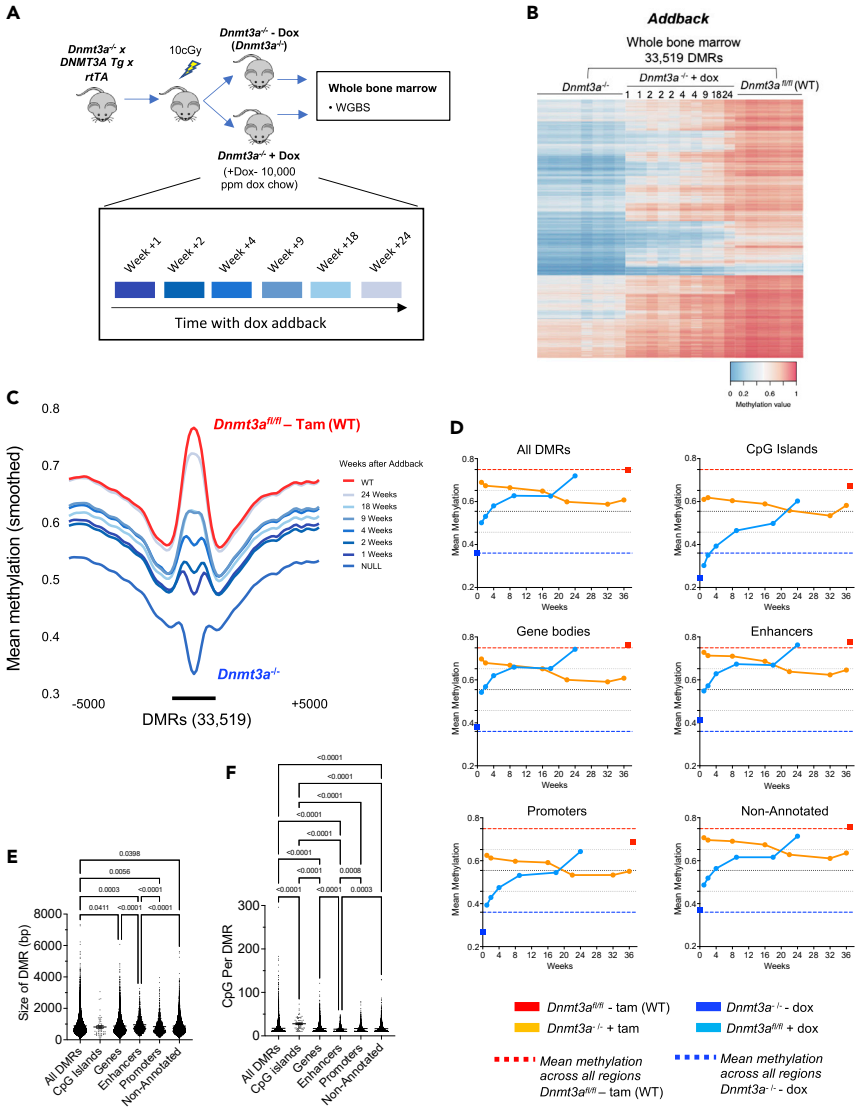

Figure 3. Methylation gain following *DNMT3A* addback is time dependent and rapid

(A) Schematic representation of the *DNMT3A* addback experiment. Dox, doxycycline; WGBS, whole genome bisulfite sequencing.

(B) Heatmap of mean methylation values for 33,519 DMRs identified by comparing *Dnmt3a*$^{fl/fl}$ – Tam (WT) vs. *Dnmt3a*$^{-/-}$ (without dox; null), with mean methylation values for dox-treated addback samples, plotted passively. Time of dox (addback) treatment is shown in weeks.

(C) Methylation density of 33,519 DMRs defined in (B), in *Dnmt3a*$^{-/-}$ + Dox samples obtained at different timepoints. Data are presented as means over all DMRs and all samples from each treatment group: *Dnmt3a* $^{-/-}$ (N = 8), *Dnmt3a*$^{fl/fl}$ + Tam (N = 6), and addback weeks 1 (N = 2), 2 (N = 3), 4 (N = 2), 9 (N = 1), 18 (N = 1), 24 (N = 1).

(D) Mean methylation values for all 33,519 DMRs and DMRs exclusive to specific annotated genomic regions are shown. The red dotted line indicates mean methylation value of all DMRs in *Dnmt3a*$^{fl/fl}$ – Tam (WT), blue dotted line indicates mean methylation value of all DMRs in *Dnmt3a*$^{-/-}$, red square indicates mean methylation value of DMRs in specified annotated region for *Dnmt3a*$^{fl/fl}$ – Tam (WT), blue square data point indicates mean methylation value of DMRs in specified annotated region for *Dnmt3a*$^{-/-}$. For quartile calculations, *Dnmt3a*$^{fl/fl}$ - Tam (red dotted line) and *Dnmt3a*$^{-/-}$ (blue dotted line) were defined as 100% and 0% methylation, respectively, and quartiles are represented by black dotted lines. Mean methylation values for all *Dnmt3a*$^{fl/fl}$ + Tam (orange line) and *Dnmt3a*$^{-/-}$ + Dox (pale blue line) over time in weeks. Data are presented as means over all DMRs in each annotated category and all samples from each treatment group: *Dnmt3a* $^{-/-}$ (N = 8), *Dnmt3a*$^{fl/fl}$ + Tam (N = 6), and addback weeks 1 (N = 2), 2 (N = 3), 4 (N = 2), 9 (N = 1), 18 (N = 1), 24 (N = 1).

(E) Size in bp (+/− Std Dev) of all 33,519 DMRs and DMRs exclusive to specific annotated genomic regions.

Figure 3. *Continued*

(F) CpGs per DMR for all 33,519 DMRs and DMRs exclusive to specific annotated genomic regions. Hypothesis testing in (E) and (F) was performed via one-way ANOVA with Tukey's multiple comparison test between each annotated genomic region (p values are indicated for each comparison; nonsignificant values are not presented). Bp; base-pairs, DMR; differentially methylated region, Dox; doxycycline, tam; tamoxifen, WGBS; whole genome bisulfite sequencing. Time is shown in weeks.

by week 24 following addback. At the 1-week timepoint, 966/1,412 (68.4%) dynamic takeaway DMRs overlapped with the 9,412 (10.3%) dynamic addback DMRs. This overlap was magnified by week 22/24 (takeaway/addback), where 9,462/9,838 (96.2%) dynamic takeaway DMRs overlapped with 29,310 (32.3%) dynamic addback DMRs (Figure 4B). We classified the dynamic DMRs identified at week-1 as *fast*, because of the rapidity with which they gain and lose methylation. An example of a fast dynamic DMR in the *Meis1* gene is shown in Figure 4C. Together, these data show that methylation gain and loss is canonical and ordered, implying that there are undefined factors that determine the rate of methylation loss at specific CpGs.

Contributions of DNA methylases and demethylases to methylation remodeling in hematopoietic cells

We next attempted to define the genes and pathways that are the most strikingly affected by fast dynamic DMRs. Defining the specific gene targets of DMR dysregulation is complex, because the proximity of a DMR to a gene does not reliably predict an effect on its expression (Spencer et al., 2017; Ketkar et al., 2020). Therefore, we interrogated dynamic vs. non-dynamic DMRs (both from week 1, and from week 22), and linked these DMRs to genes in two different ways: first, we required a DMR to be mapped to a gene promoter, gene body, or anywhere within 10 kb of a gene. The second analysis was more restrictive, requiring the DMR to map to a gene's promoter. Using these definitions, we performed gene ontology analysis to determine whether specific pathways related to GO biological processes were significantly enriched (DMR locations, genomic annotation, and enrichment analyses are found in Table S3, and graphical representations of the enrichment analyses are in Figures S1 and S2). Using a false-discovery-rate cutoff of 0.001, several pathways were enriched in the dynamic DMRs with both analyses, and at both timepoints; the GO terms for these pathways were extraordinarily diverse, and were difficult to connect to processes thought to be related to altered self-renewal and/or differentiation in Dnmt3a deficient hematopoietic cells. Clearly, additional studies will be required to better understand the physiologic consequences associated with fast vs. slow methylation loss at specific loci.

We explored the hypothesis that the slow loss of methylation with takeaway may also be influenced by the slow rates of hematopoietic stem/progenitor cell (HSPC) division, with passive methylation loss as cells repeatedly divide. Because *Dnmt3a* is primarily expressed in HSPCs (Ketkar et al., 2020; Tadokoro et al., 2007), methylation patterns may be established by Dnmt3a in HSPCs, maintained during subsequent cell divisions by Dnmt1, and remodeled by the Tet demethylases as cells commit to terminal differentiation. We tested this hypothesis by comparing the methylomes of unfractionated whole bone marrow cells, purified progenitor populations (KLS, CMP, GMP, and MEP; data grouped for analysis), and mature lineage populations (myeloid, B-cells, or T-cells). By comparing WGBS data from mature myeloid cells (CD11b+/Gr1+) to the progenitor populations of WT mice, we identified 574 DMRs (Figure 5A), of which 552 (96.2%) were hypomethylated in the mature myeloid cells; this supports the hypothesis that the Tet demethylases may actively remodel the methylome during lineage commitment. Passively plotting B-cell and T-cell WGBS data against the myeloid-defined DMRs showed that these regions are specific to the mature myeloid cells, retaining a progenitor-like signature in lymphoid cells. In addition, because myeloid cells are a major population in unfractionated whole bone marrow, the mature myeloid signature was also apparent in those samples. More committed GMPs were more hypomethylated than CMPs and MEPs, suggesting that remodeling is initiated before terminal differentiation, and may therefore play a role in commitment. Likewise, we identified specific B-cell (Figure S3A) and T-cell (Figure S3B) DMRs, which were methylated in myeloid cells.

Only 57/574 (10.3%) mature myeloid DMRs were detected in the 33,519 *Dnmt3a* dependent DMRs defined in Figure 1D (Figure 5B). In contrast, 416/2,031 (20.5%) B-cell DMRs and 619/2,271 (27.3%) T-cell DMRs overlapped with the 33,519 Dnmt3a$^{-/-}$ DMRs (Figures S3A–S3D). Passive plotting of the progenitor and mature lineage populations from *Dnmt3a*$^{+/+}$ mice against the 33,519 *Dnmt3a*$^{-/-}$ DMRs confirmed that these

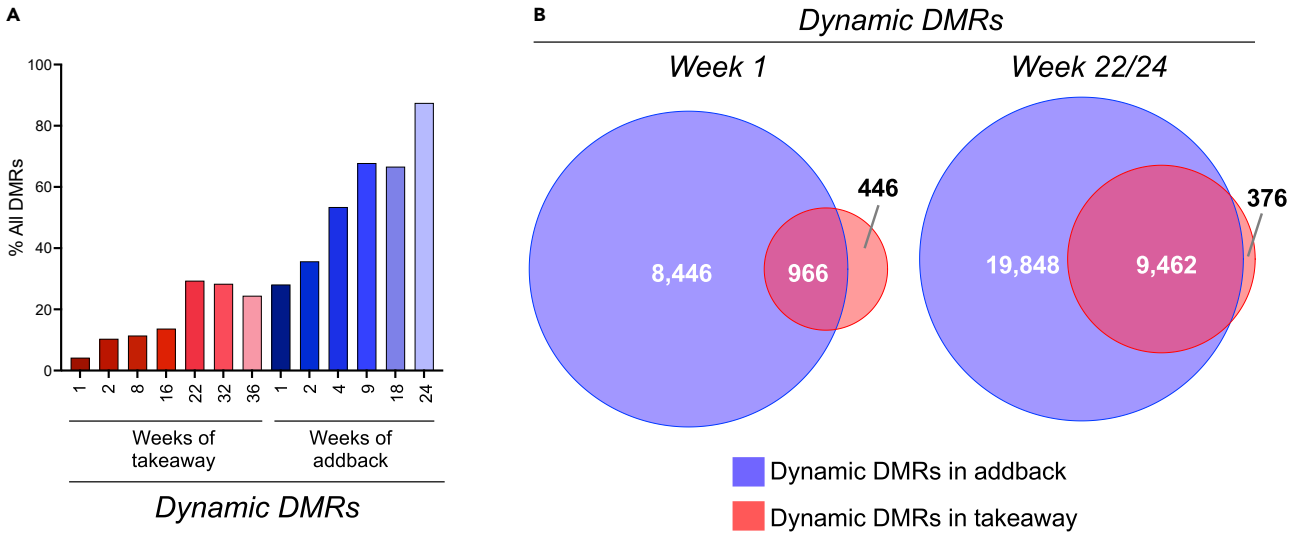

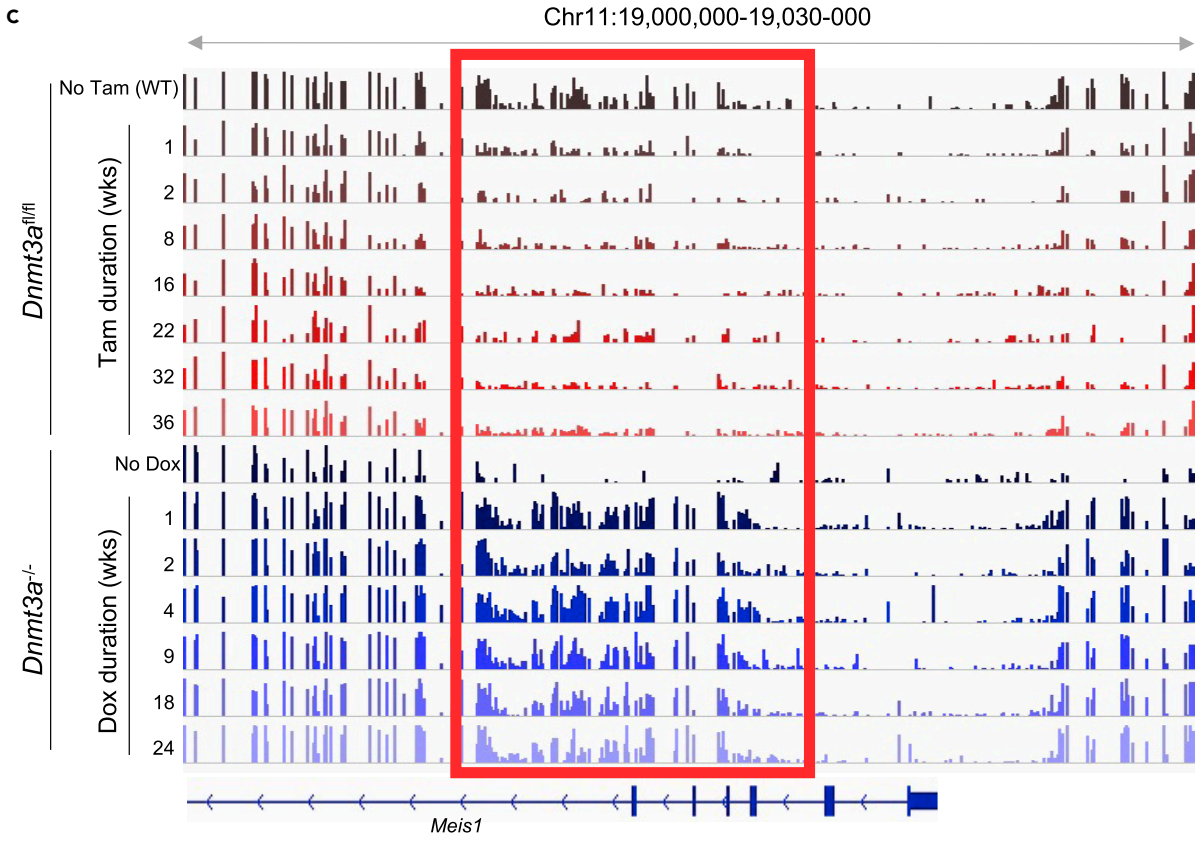

Figure 4. Characteristics of dynamic DMRs

(A) Percent of DMRs that are dynamic at each time point in the whole bone marrow from *Dnmt3a*$^{fl/fl}$ + Tam (takeaway) and *Dnmt3a*$^{-/-}$ + Dox (addback) mice. Dynamic DMRs are defined as those that have a change in beta value of >0.2 from baseline where baseline for takeaway and addback are defined as values in *Dnmt3a*$^{fl/fl}$ – Tam (WT) and *Dnmt3a*$^{-/-}$ for individual DMRs, respectively.

(B) Venn diagram showing overlap between dynamic DMRs identified in *Dnmt3a*$^{fl/fl}$ + Tam (takeaway; red) and *Dnmt3a*$^{-/-}$ + Dox (addback; blue) mice at week 1, and at weeks 22/24. The dynamic DMRs found in week 1 are classified as *rapid* dynamic DMRs.

Figure 4. *Continued*
(C) Example of a *rapid* dynamic DMR within the *Meis1* gene. The gene structure is shown below, genomic location (assembly mm10) shown above, individual CpGs are represented by colored bars, y -axis is mean methylation of CpGs, time is given in weeks, and the DMR is highlighted in the gray box. DMR; differentially methylated region, Dox; doxycycline, tam; tamoxifen. Time is shown in weeks.

Dnmt3a dependent regions are almost mutually exclusive from the majority of myeloid-specific remodeling sites (Figure S3E). As expected, the 6,435 DMRs defined in the earliest progenitors (KLS and CMP) were persistent in the GMP and MEP compartments, and also in whole bone marrow samples (Figure S4); this suggests that the methylation events mediated by Dnmt3a in HSPCs must be maintained throughout hematopoietic differentiation by Dnmt1 (Ketkar et al., 2020). In aggregate, these data suggest that lineage-specific methylation remodeling during hematopoietic differentiation must primarily depend on the actions of the Tet proteins, and not the actions of Dnmt3a or 3b in more mature cells (Farlik et al., 2015, 2016).

This hypothesis is also supported by single cell RNA sequencing data from unfractionated whole bone marrow and lineage-depleted, Kit positive (Lin-Kit+; LK) cells from WT mice (Ketkar et al., 2020). *Dnmt3a* and *Dnmt3b* are expressed in almost a third of all LK cells, but in less than 1% of mature myeloid and monocytic cells (PMN and Mono; Figures 5C–5E). Although *Tet1* expression follows the same pattern, *Tet2* and *3* gene expressions persist in the mature populations, suggesting they may play a more active role in methylome remodeling during differentiation (Figures 5D and 5E). Combined, these data suggest that the influence of Dnmt3a on the methylome is largely restricted to HSPCs; because these cells divide slowly and comprise only a tiny fraction of the bone marrow, this may help to explain, at least in part, the slow rate of methylation loss detected in the whole bone marrow samples.

DISCUSSION

In this report, we describe the kinetics of DNA methylation loss following the inactivation of *Dnmt3a* in hematopoietic cells *in vivo*. A canonical, ordered pattern of DNA methylation loss was observed in bone marrow cells following *Dnmt3a* floxing, as early as one-week after a 3 weeks treatment course of Tamoxifen, and with progressive loss over the following 35 weeks. Even at the final time point, mean levels of methylation did not reach half that of DMRs defined in the bone marrow cells of Dnmt3a knockout mice. This contrasts to the speed of methylation gain following re-expression of physiologic levels of DNMT3A in constitutive null bone marrow cells, where a significant fraction of DMRs are remethylated within a week of initiating addback (Ketkar et al., 2020). Further, 94% of knockout DMRs are remethylated (to within 20% of *Dnmt3a*-WT values) by week 24 of addback. The contrasting kinetics of Dnmt3a dependent methylation loss and gain were highlighted by assessing dynamic DMRs (i.e., those DMRs that had a change in beta values of $\geq$ 0.2 from their baselines at a specific timepoint). Rapidly changing, dynamic DMRs with takeaway or addback had significant overlap, suggesting that *Dnmt3a* is active at very specific genomic sites. Taken together, these data suggest that the loss of DNA methylation following somatic Dnmt3a inactivation in hematopoietic cells is canonical and slow, and may take years to develop fully.

Several studies have evaluated aspects of DNA methylation changes after Dnmt3a inactivation *in vivo* (Challen et al., 2011, 2014; Jeong et al., 2018). For example, a study of serial transplantation of hematopoietic stem cells from young Dnmt3a flox/flox mice with Mx1-Cre (treated with polyI:polyC), showed that significant methylation loss (i.e., 5,000 DMRs) could be detected after three serial passages *in vivo* (over a period of about 4 months, faster than the timeframe of this study), which progressed with additional rounds of serial transplantation over a period of nearly two years (Jeong et al., 2018). The rate of methylation loss in that study may have been accelerated by serial transplantation, which places HSCs under proliferative stress, as they undergo repeated rounds of enforced repopulation of the hematopoietic system. In addition, Dnmt3a deficient HSCs have a competitive advantage in this model system, which may accelerate the apparent rate of methylation loss. Based on that study and our observations, we suggest that a high rate of HSC division may accelerate 'passive' methylation loss in the absence of Dnmt3a, as a consequence of extra HSC cell divisions. In contrast, the model used in the current study more closely resembles the events expected to transpire after somatic *DNMT3A* mutations occur in the HSPCs of humans, because both may have steady state hematopoiesis at the time that the mutation occurs (Ketkar et al., 2020; Smith et al., 2021). Indeed, patients with clonal hematopoiesis, and those with germline mutations in *DNMT3A* (DNMT3A Overgrowth Syndrome) can have relatively unperturbed blood cell counts and hematopoiesis for many years (or even decades) before transformation (Smith et al., 2021; Jaiswal et al., 2014).

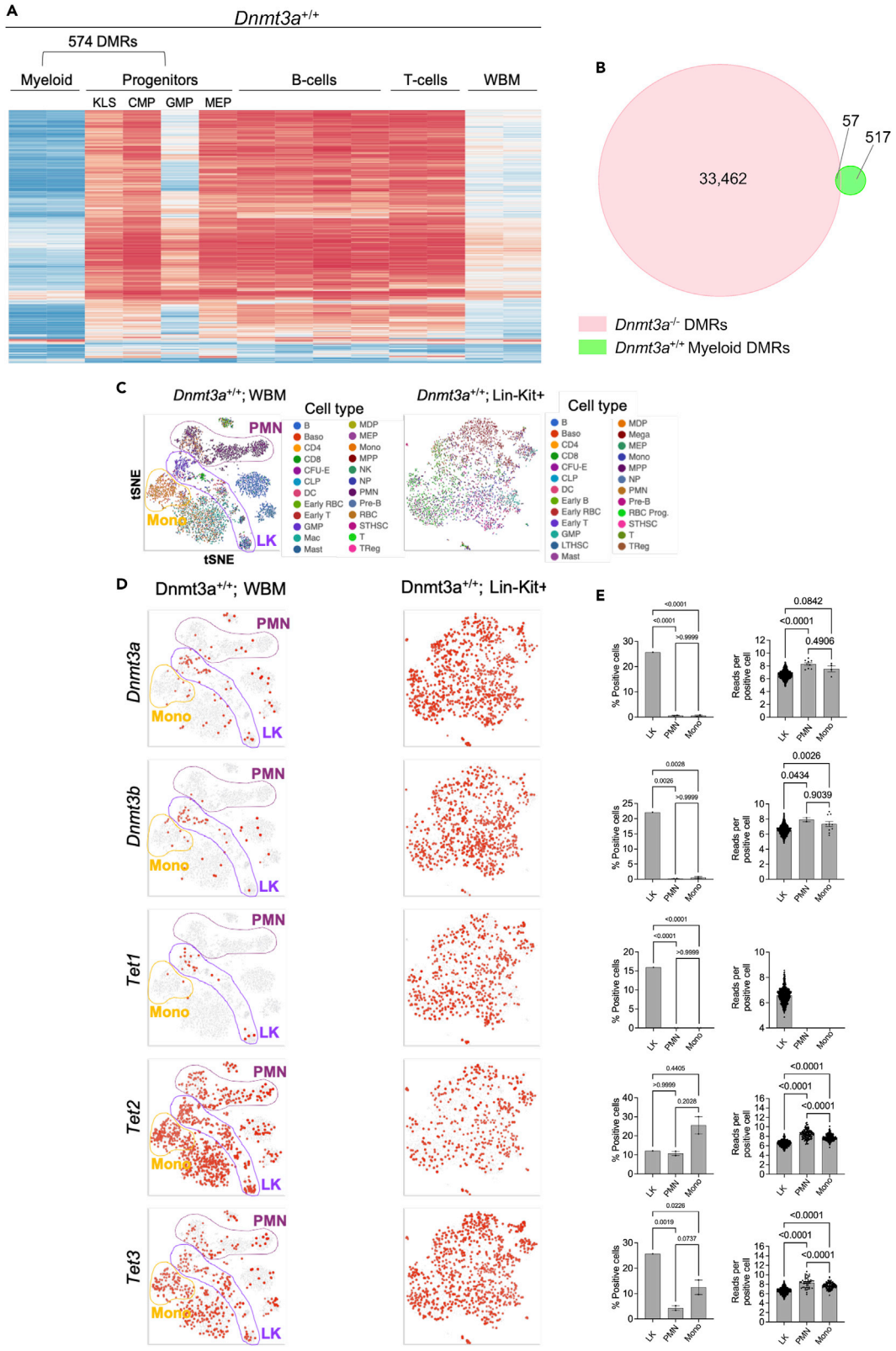
A
Dnmt3a+/+
574 DMRs
Myeloid
Progenitors
KLS CMP GMP MEP
B-cells
T-cells
WBM
B
33,462
57
517
Dnmt3a-/- DMRs
Dnmt3a+/+ Myeloid DMRs
C
Dnmt3a+/+; WBM
Cell type
Dnmt3a+/+; Lin-Kit+
Cell type
tSNE
PMN
Mono
LK
D
Dnmt3a+/+; WBM
Dnmt3a+/+; Lin-Kit+
Dnmt3a
Dnmt3b
Tet1
Tet2
Tet3
E
% Positive cells
Reads per positive cell
LK
PMN
Mono

Figure 5. Differential methylation and expression signatures in hematopoietic progenitors vs. mature myeloid cells

(A) Heatmap of mean methylation values for DMRs identified by comparing flow-purified progenitors (KLS, MEP, CMP, and GMP; grouped for analysis) and mature myeloid cells (CD11b+/Gr1+) isolated by FACS sorting. Methylation values for those DMRs in B-cells, T-cells, and whole bone marrow are passively plotted.

(B) Venn diagram showing overlap of the 33,519 DMRs defined in *Dnmt3a*$^{-/-}$ bone marrow vs. the 574 DMRs from *Dnmt3a*$^{+/+}$ myeloid cells. Overlap between DMRs is defined as a minimum of 1 bp.

(C) tSNE projections of scRNA-seq data from whole bone marrow (*left*) and lineage depleted, Kit positive (Lin-Kit+) progenitor cells (*right*) purified by FACS. Mature neutrophils (PMN), monocytes (mono), and lineage negative, KIT positive cells (LK) are highlighted on the whole bone marrow projection.

(D) Cells are colored according to levels of expression of *Dnmt3a*, *Dnmt3b*, *Tet1*, *Tet2,* and *Tet3* (top to bottom) in *Dnmt3a*$^{+/+}$ whole bone marrow (*left* panels) or lineage negative c-Kit positive cells (*right* panels).

(E) Quantitation of percent total cells positive for expression (*left* panels) and number of normalized reads per positive cell (*right* panels) for *Dnmt3a*, *Dnmt3b*, *Tet1*, *Tet2,* and *Tet3* genes in the indicated cell type. LK; lineage negative, c-KIT positive, WBM; whole bone marrow. One-way ANOVA testing was used to define statistical differences between groups. For *Tet1*, no reads were detected in the PMNs and Monos, so statistical comparisons could not be performed.

Although the factors that contribute to the rate of DNA methylation loss after somatic inactivation of Dnmt3a in steady state hematopoiesis are unclear, they are almost certainly influenced by the relative activities of DNA methyltransferases and demethylases during different stages of hematopoietic development. Maintenance of the methylome involves a network of DNA methyltransferases (DNMT1, DNMT3A, and DNMT3B) that add methylation marks to specific CpG residues in the genome, and a set of enzymes that act to demethylate CpGs (TET1, TET2, TET3). The discovery of the TET enzymes has implied that DNA demethylation is an active, regulated process that shapes DNA methylation patterns in the genome. The slow rate of methylation loss presented here suggests that Tet-mediated demethylation may predominantly occur in genomic regions that are not methylated by Dnmt3a in hematopoietic cells. This may be related to the role of Tet-mediated demethylation in the commitment and differentiation of myeloid cells (Ostrander et al., 2020). Izzo et al. (2020) used conditional knockout models to identify the opposing roles of Tet2 and Dnmt3a in myelomonocytic and erythroid lineage differentiation, respectively, which were related to CpG enrichment in the DNA binding motifs of cell fate-determining transcription factors (Izzo et al., 2020). Further, we have shown that mice that are constitutively null for *Dnmt3a* display an expansion of myeloid cells over time, at the expense of the lymphoid lineage (Ketkar et al., 2020). This myeloid expansion was directly linked to *Dnmt3a* deficiency and focal hypomethylation, because *DNMT3A* addback restored methylation and reduced myeloid skewing and restored lymphoid populations (Ketkar et al., 2020). Further, we suggest that it is probably the activity of demethylases, not methyltransferases that define the unique methylomes of the mature myeloid compartment. The DMRs defined in Dnmt3a null mice vs. myeloid-specific DMRs are nearly mutually exclusive; this supports the idea that remodeling that drives differentiation is not occurring in the same sites where Dnmt3a is active. In contrast, lymphoid lineages have more differentiation-dependent DMRs that overlap with Dnmt3a DMRs. Tadokoro et al. likewise showed that Dnmt3a expression is high in lymphoid cells from the spleen and thymus (sites of B-cell and T-cell maturation), compared to mature myeloid cells from bone marrow (Tadokoro et al., 2007). Further, conditional knockout of *Dnmt3a* in Lineage-/Kit-/Sca1-/CD34- cells from Dnmt3a$^{flox/flox}$ mice, did not impair peripheral blood chimerism, but led to reductions in B- and T-cell chimerism compared to non-floxed controls. Again, this suggests that expression of Dnmt3a and maintenance of Dnmt3a-dependent methylation is required for the differentiation of lymphoid cells (Tadokoro et al., 2007). Finally, the conditional knockout of both Dnmt3a and Dnmt3b was shown to impair B-cell differentiation, which is mediated at least in part by an increase in ß-catenin signaling (Challen et al., 2014). The competition between the methyltransferase and demethylase enzymes, and their expression levels at different stages of development, probably play a major role in methylome remodeling during hematopoietic development.

Additional studies suggest that *Dnmt3b* can act in the stead of *Dnmt3a* after it is deleted, perhaps slowing methylation loss, but not preventing it entirely. In support of this idea, a recent study performed in human embryonic stem cells showed that differentially methylated regions (defined by *DNMT3A*/*DNMT3B* double knockouts) retained 93% of WT methylation values when only one of the *DNMT3* genes was deleted. Further, when TET knockout preceded *DNMT3A /DNMT3B* double knockout, methylation levels did not progressively fall, even after 20 passages (Charlton et al., 2020). It remains to be determined whether the same rules apply to hematopoietic stem cells, lineage committed progenitors, and terminally differentiated cells. Although a 'methyltransferase-dead' splicing variant of *Dnmt3b* (*Dnmt3b3*) is the most abundant in mouse (and human) hematopoietic cells, some *Dnmt3b1* is expressed and is active, as manifest by the more severe methylation phenotype of Dnmt3a × Dnmt3b double knockout mice (Challen et al., 2014). Further, recent

evidence suggests that Dnmt3b3 can directly interact with Dnmt3a to increase its activity (Xu et al., 2020; Zeng et al., 2020). Combined, these data suggest that the methyltransferase activities of DNMT3A and B are somewhat redundant, and that one can maintain methylation in the absence of the other.

Somatic mutations in *DNMT3A* are common in acute myeloid leukemia and associated with a focal, canonical hypomethylation phenotype (Spencer et al., 2017). Recent data from patients with germline mutations in *DNMT3A* (DNMT3A Overgrowth Syndrome) have shown that the hypomethylation phenotype develops in the hematopoietic cells in very young patients with relatively normal blood counts (Smith et al., 2021). However, studies from patients with clonal hematopoiesis show that there is an increased risk of malignancy in these patient cohorts (Genovese et al., 2014; Jaiswal et al., 2014; Xie et al., 2014), and emerging data suggests the same is true for DNMT3A Overgrowth Syndrome patients (Smith et al., 2021). Although previous studies have suggested that the hypomethylation phenotype may be in part responsible for the increased fitness of these cells for transformation, the connection between the mutational event and overt disease has been difficult to understand because of the long latency of the premalignant state. The data from this study suggests that the slow methylation loss after Dnmt3a inactivation may be another contributing factor to long latency in clonal hematopoiesis patients, and that interventions designed to reactivate or restore DNMT3A activity during this latent period may be therapeutically attractive.

Limitations of the study

All of the experiments of this study were performed in mice; hence, the kinetics of DNA methylation loss in human hematopoietic cells that acquire loss-of-function mutations in *DNMT3A* can only be estimated from these data. Because we measured DNA methylation loss in single animals at different time points after *Dnmt3a* inactivation, it was not possible to define statistical differences among DMRs at individual time points in the experiment; only trends could be discerned. The model system used (homozygous inactivation of *Dnmt3a*) was chosen to accentuate methylation findings; in contrast, human AML patients almost always have heterozygous *DNMT3A* inactivating mutations, or dominant negative mutations (at amino acid R882) that reduce DNMT3A activity by ~80%. Finally, we currently have a limited understanding of the factors that influence DNA methylation remodeling during hematopoietic development, and how these factors may contribute to patterns of methylation loss after somatic inactivation of *DNMT3A* in humans.

STAR★METHODS

Detailed methods are provided in the online version of this paper and include the following:

- KEY RESOURCES TABLE
- RESOURCE AVAILABILITY
  - Lead contact
  - Materials availability
  - Data and code availability
- EXPERIMENTAL MODEL AND SUBJECT DETAILS
  - *Dnmt3a*$^{fl/fl}$ -ER^{TM}-cre mice
  - *Dnmt3a*$^{-/-}$ x rtTA x WT *DNMT3A* mice
- METHOD DETAILS
  - Collection and processing of whole bone marrow
  - Floxing efficiency assay
  - Whole-genome bisulfite sequencing
  - FACS sorting of cell populations
  - Single cell RNA sequencing
- QUANTIFICATION AND STATISTICAL ANALYSIS

SUPPLEMENTAL INFORMATION

Supplemental information can be found online at https://doi.org/10.1016/j.isci.2022.104004.

ACKNOWLEDGMENTS

The authors thank Ms. Mieke Hoock for excellent animal husbandry. This work was supported by an ASH Fellow to Faculty Award (A.M.S.), NIH grants CA237727 (D.Y.C.), CA211782 (C.A.M.), CA101937 and CA197561 (T.J.L.), and the Barnes-Jewish Hospital Foundation (T.J.L.).

AUTHOR CONTRIBUTIONS

A.M.S., A.M.V., and T.J.L. designed research. A.M.S., A.M.V., D.Y.C., and E.R.L. performed research. A.M.S., H.J.A., S.K., and C.A.M., analyzed the data. A.M.S. and T.J.L. wrote the paper.

DECLARATION OF INTERESTS

A.M.S. is an employee of Incyte Corporation, A.M.V. is an employee of Vitalant Corporation, and E.R.L. is the owner of Leight Medical Communications, LLC. All studies in the manuscript were performed before the authors joined these companies. The other authors declare no competing interests.

Received: October 13, 2021
Revised: February 17, 2022
Accepted: February 24, 2022
Published: April 15, 2022

REFERENCES

Challen, G.A., Sun, D., Jeong, M., Luo, M., Jelinek, J., Berg, J.S., Bock, C., Vasanthakumar, A., Gu, H., Xi, Y., et al. (2011). Dnmt3a is essential for hematopoietic stem cell differentiation. Nat. Genet. *44*, 23–31.

Challen, G.A., Sun, D., Mayle, A., Jeong, M., Luo, M., Rodriguez, B., Mallaney, C., Celik, H., Yang, L., Xia, Z., et al. (2014). Dnmt3a and Dnmt3b have overlapping and distinct functions in hematopoietic stem cells. Cell Stem Cell *15*, 350–364.

Charlton, J., Jung, E.J., Mattei, A.L., Bailly, N., Liao, J., Martin, E.J., Giesselmann, P., Brandl, B., Stamenova, E.K., Muller, F.J., et al. (2020). TETs compete with DNMT3 activity in pluripotent cells at thousands of methylated somatic enhancers. Nat. Genet. *52*, 819–827.

Cole, C.B., Russler-Germain, D.A., Ketkar, S., Verdoni, A.M., Smith, A.M., Bangert, C.V., Helton, N.M., Guo, M., Klco, J.M., O'laughlin, S., et al. (2017). Haploinsufficiency for DNA methyltransferase 3A predisposes hematopoietic cells to myeloid malignancies. J. Clin. Invest. *127*, 3657–3674.

de Graaf, C.A., Choi, J., Baldwin, T.M., Bolden, J.E., Fairfax, K.A., Robinson, A.J., Biben, C., Morgan, C., Ramsay, K., Ng, A.P., et al. (2016). Haemopedia: an expression atlas of murine hematopoietic cells. Stem Cell Rep. *7*, 571–582.

Farlik, M., Sheffield, N.C., Nuzzo, A., Datlinger, P., Schonegger, A., Klughammer, J., and Bock, C. (2015). Single-cell DNA methylome sequencing and bioinformatic inference of epigenomic cell-state dynamics. Cell Rep. *10*, 1386–1397.

Farlik, M., Halbritter, F., Muller, F., Choudry, F.A., Ebert, P., Klughammer, J., Farrow, S., Santoro, A., Ciaurro, V., Mathur, A., et al. (2016). DNA methylation dynamics of human hematopoietic stem cell differentiation. Cell Stem Cell *19*, 808–822.

Gaidzik, V.I., Schlenk, R.F., Paschka, P., Stolzle, A., Spath, D., Kuendgen, A., Von Lilienfeld-Toal, M., Brugger, W., Derigs, H.G., Kremers, S., et al. (2013). Clinical impact of DNMT3A mutations in younger adult patients with acute myeloid leukemia: results of the AML Study Group (AMLSG). Blood *121*, 4769–4777.

Gale, R.E., Lamb, K., Allen, C., El-Sharkawi, D., Stowe, C., Jenkinson, S., Tinsley, S., Dickson, G., Burnett, A.K., Hills, R.K., and Linch, D.C. (2015). Simpson's paradox and the impact of different DNMT3A mutations on outcome in younger adults with acute myeloid leukemia. J. Clin. Oncol. *33*, 2072–2083.

Genovese, G., Kahler, A.K., Handsaker, R.E., Lindberg, J., Rose, S.A., Bakhoum, S.F., Chambert, K., Mick, E., Neale, B.M., Fromer, M., et al. (2014). Clonal hematopoiesis and blood-cancer risk inferred from blood DNA sequence. N. Engl. J. Med. *371*, 2477–2487.

Izzo, F., Lee, S.C., Poran, A., Chaligne, R., Gaiti, F., Gross, B., Murali, R.R., Deochand, S.D., Ang, C., Jones, P.W., et al. (2020). DNA methylation disruption reshapes the hematopoietic differentiation landscape. Nat. Genet. *52*, 378–387.

Jaiswal, S., Fontanillas, P., Flannick, J., Manning, A., Grauman, P.V., Mar, B.G., Lindsley, R.C., Mermel, C.H., Burtt, N., Chavez, A., et al. (2014). Age-related clonal hematopoiesis associated with adverse outcomes. N. Engl. J. Med. *371*, 2488–2498.

Jeong, M., Park, H.J., Celik, H., Ostrander, E.L., Reyes, J.M., Guzman, A., Rodriguez, B., Lei, Y., Lee, Y., Ding, L., et al. (2018). Loss of Dnmt3a immortalizes hematopoietic stem cells *in vivo*. Cell Rep. *23*, 1–10.

Juhling, F., Kretzmer, H., Bernhart, S.H., Otto, C., Stadler, P.F., and Hoffmann, S. (2016). metilene: fast and sensitive calling of differentially methylated regions from bisulfite sequencing data. Genome Res. *26*, 256–262.

Kaneda, M., Okano, M., Hata, K., Sado, T., Tsujimoto, N., Li, E., and Sasaki, H. (2004). Essential role for de novo DNA methyltransferase Dnmt3a in paternal and maternal imprinting. Nature *429*, 900–903.

Ketkar, S., Verdoni, A.M., Smith, A.M., Bangert, C.V., Leight, E.R., Chen, D.Y., Brune, M.K., Helton, N.M., Hoock, M., George, D.R., et al. (2020). Remethylation of Dnmt3a (−/−) hematopoietic cells is associated with partial correction of gene dysregulation and reduced myeloid skewing. Proc. Natl. Acad. Sci. U S A *117*, 3123–3134.

Ley, T.J., Ding, L., Walter, M.J., Mclellan, M.D., Lamprecht, T., Larson, D.E., Kandoth, C., Payton, J.E., Baty, J., Welch, J., et al. (2010). DNMT3A mutations in acute myeloid leukemia. N. Engl. J. Med. *363*, 2424–2433.

Marcucci, G., Metzeler, K.H., Schwind, S., Becker, H., Maharry, K., Mrozek, K., Radmacher, M.D., Kohlschmidt, J., Nicolet, D., Whitman, S.P., et al. (2012). Age-related prognostic impact of different types of DNMT3A mutations in adults with primary cytogenetically normal acute myeloid leukemia. J. Clin. Oncol. *30*, 742–750.

Ostrander, E.L., Kramer, A.C., Mallaney, C., Celik, H., Koh, W.K., Fairchild, J., Haussler, E., Zhang, C.R.C., and Challen, G.A. (2020). Divergent effects of Dnmt3a and Tet2 mutations on hematopoietic progenitor cell fitness. Stem Cell Rep. *14*, 551–560.

Renneville, A., Boissel, N., Nibourel, O., Berthon, C., Helevaut, N., Gardin, C., Cayuela, J.M., Hayette, S., Reman, O., Contentin, N., et al. (2012). Prognostic significance of DNA methyltransferase 3A mutations in cytogenetically normal acute myeloid leukemia: a study by the Acute Leukemia French Association. Leukemia *26*, 1247–1254.

Russler-Germain, D.A., Spencer, D.H., Young, M.A., Lamprecht, T.L., Miller, C.A., Fulton, R., Meyer, M.R., Erdmann-Gilmore, P., Townsend, R.R., Wilson, R.K., and Ley, T.J. (2014). The R882H DNMT3A mutation associated with AML dominantly inhibits wild-type DNMT3A by blocking its ability to form active tetramers. Cancer Cell *25*, 442–454.

Smith, A.M., Lavalle, T.A., Shinawi, M., Ramakrishnan, S.M., Abel, H.J., Hill, C.A., Kirkland, N.M., Rettig, M.P., Helton, N.M., Heath, S.E., et al. (2021). Functional and epigenetic phenotypes of humans and mice with DNMT3A overgrowth syndrome. Nat. Commun. *12*, 4549.

Spencer, D.H., Russler-Germain, D.A., Ketkar, S., Helton, N.M., Lamprecht, T.L., Fulton, R.S., Fronick, C.C., O'laughlin, M., Heath, S.E., Shinawi, M., et al. (2017). CpG island hypermethylation mediated by DNMT3A is a consequence of AML progression. Cell *168*, 801–816.e13.

Tadokoro, Y., Ema, H., Okano, M., Li, E., and Nakauchi, H. (2007). De novo DNA methyltransferase is essential for self-renewal, but not for differentiation, in hematopoietic stem cells. J. Exp. Med. *204*, 715–722.

Xie, M., Lu, C., Wang, J., Mclellan, M.D., Johnson, K.J., Wendl, M.C., Mcmichael, J.F., Schmidt, H.K., Yellapantula, V., Miller, C.A., et al. (2014). Age-related mutations associated with clonal hematopoietic expansion and malignancies. Nat. Med. *20*, 1472–1478.

Xu, T.H., Liu, M., Zhou, X.E., Liang, G., Zhao, G., Xu, H.E., Melcher, K., and Jones, P.A. (2020). Structure of nucleosome-bound DNA methyltransferases DNMT3A and DNMT3B. Nature *586*, 151–155.

Zeng, Y., Ren, R., Kaur, G., Hardikar, S., Ying, Z., Babcock, L., Gupta, E., Zhang, X., Chen, T., and Cheng, X. (2020). The inactive Dnmt3b3 isoform preferentially enhances Dnmt3b-mediated DNA methylation. Genes Dev. *34*, 1546–1558.

STAR★METHODS

KEY RESOURCES TABLE

REAGENT or RESOURCE	SOURCE	IDENTIFIER
Antibodies		
CD11b (MI/70)	Becton Dickinson	565080; RRID: AB_2722548
Gr1 (TB6-8C5)	Biolegend	108456; RRID: AB_2616737
Ter-119 (Ter119)	Becton Dickinson	740875; RRID: AB_2740526
CD71 (C2)	Becton Dickinson	563013; RRID: AB_2737950
B220 (RA3-6B2)	Becton Dickinson	612950; RRID: AB_2870227
CD3e (145-2C11)	Becton Dickinson	564618; RRID: AB_2738868
Sca-1 (D7)	Biolegend	108138; RRID: AB_2564042
c-KIT (2B8)	Becton Dickinson	562609; RRID: AB_11154585
CD34 (RAM34)	Becton Dickinson	553733; RRID: AB_395017
FLT3 (A2F10)	Biolegend	135306; RRID: AB_1877217
CD150 (TC15-12F12.2)	Biolegend	115941; RRID: AB_2629660
CD48 (HM48-1)	Biolegend	103420; RRID: AB_1089037
CD45.1 (A20)	Becton Dickinson	563983; RRID: AB_2738523
CD45.2 (104)	Becton Dickinson	740131; RRID: AB_2739888
Chemicals, peptides, and recombinant proteins		
Ammonium Chloride/KCl (ACK) red cell lysis buffer	Sigma	A9434, P9541
SYBR green	Thermo Fisher	K0221
RPMI media	Gibco	11875034
15% FBS	Atlanta Biologicals	S11550H
Tamoxifen	Sigma	T5648
Critical commercial assays		
Chromium Single Cell 5′ Kits	10x Genomics	#1000286, #1000263, #1000215
Accel NGS Methyl-Seq DNA library kit	Swift Biosciences	#30096
Deposited data		
Aligned Sequence Data	This paper	NCBI: PRJNA797693
Experimental models: Organisms/strains		
C57Bl/6-CD45.1 (NCI B6-Ly5.1/Cr)	Charles River Laboratories.	564
C57Bl/6-CD45.2 *Dnmt3a*$^{fl/fl}$ -ER^{TM}-cre mice (B6.Cg-Tg(CAG-cre/Esr1*)5Amc/J	Jackson Labs	004682
Oligonucleotides		
Actin F1 primer: 5′-CGGGCTGTATTCCCCTCCATCG-3′	this paper	N/A
Actin R1 primer: 5′-GCCATGTTCAATGGGGTACTTCAGGG-3′	this paper	N/A
Dnmt3a F1 primer: 5′-CGGTCATTCCAGATGATTCCTC-3′	this paper	N/A
Dnmt3a R1 primer: 5′-TGCTGTGGATGT-AGGAAAGCTG-3′	this paper	N/A
Software and algorithms		
WGBS analysis pipeline	https://github.com/genome/analysis-workflows/blob/master/definitions/pipelines/	bisulfite.cwl
RNA-seq analysis pipeline	https://github.com/genome/analysis-workflows/blob/master/definitions/pipelines/	rnaseq.cwl

(*Continued on next page*)

Continued

REAGENT or RESOURCE	SOURCE	IDENTIFIER
Metilene	Juhling et al., 2016	v0.2.6; quay.io/biocontainers/metilene:0.2.6–h470a237_1
Partek Flow	Partek, Inc.,	build 10.0.21.0411
CellRanger	10X Genomics	v3.1
Winlist	Verity Software House	version 8
Other		
10,000 ppm doxycycline chow	Gateway Lab Supply	1815461-203
EDTA capillary tubes	Sarstetdt	20.1278.100

RESOURCE AVAILABILITY

Lead contact

Further information and requests for resources and reagents should be directed to and will be fulfilled by the lead contact, Timothy J. Ley (timley@wustl.edu)

Materials availability

This study did not generate new unique reagents.

Data and code availability

- Sequencing data for all mouse datasets were deposited to the NCBI: NCBI BioProject PRJNA797693 (https://www.ncbi.nlm.nih.gov/bioproject/797693), and are available without restrictions. Data from previously published work from our group that are included in this study were deposited to the NCBI, https://www.ncbi.nlm.nih.gov/bioproject/483874 (BioProject ID PRJNA483874).
- All pipeline code used for genomic data processing is available at https://github.com/genome/analysis-workflows (commit id: 174f3b2). The alignment and expression quantification workflow is described in pipelines/rnaseq.cwl, and bisulfite alignment and methylation inference is described in pipelines/bisulfite.cwl. Haemopedia expression atlas cell lineage assignment code is available at https://github.com/genome/docker-scrna_lineage_inference.
- Any additional information required to reanalyze the data reported in this paper is available from the lead contact upon request.

EXPERIMENTAL MODEL AND SUBJECT DETAILS

Animal procedures were approved by the Washington University Institutional Animal Care and Use Committee (IACUC) and conducted in accordance with all institutional guidelines.

Dnmt3a$^{fl/fl}$ -ER^{TM}-cre mice

Bone marrow from 6 week old male C57Bl/6-CD45.2 *Dnmt3a*$^{fl/fl}$ -ER^{TM}-cre mice (B6.Cg-Tg(CAG-cre/Esr1*)5Amc/J Jackson Labs 004682) was transplanted into lethally irradiated male C57Bl/6-CD45.1 recipients, and allowed to engraft for 4 weeks. Engraftment was assessed 4 weeks post-transplant by flow cytometric determination of the ratio of CD45.1 (recipient; clone A20; Becton Dickinson) to CD45.2 (donor; clone 104, Becton Dickinson) in the peripheral blood of recipient mice. Peripheral blood was obtained from the retro-orbital space with EDTA capillary tubes (Fisher Scientific) after adequate anesthesia with 2-Chloro-2-(difluoromethoxy)-1,1,1-trifluoroethane. Engraftment frequencies of >80% were detected in virtually all mice. Inactivation of *Dnmt3a* in mice transplanted with C57Bl/6-CD45.2 *Dnmt3a*$^{fl/fl}$ -ER^{TM}-cre bone marrow was induced with 9 doses of Tamoxifen (4 mg per dose per mouse in corn oil; Sigma) given by gavage on Monday, Wednesday, and Friday of each week for three consecutive weeks.

Dnmt3a$^{-/-}$ x rtTA x WT *DNMT3A* mice

Bone marrow from *Dnmt3a*$^{-/-}$ mice containing a tetracycline—inducible, WT human *DNMT3A1* cDNA (*Dnmt3a*$^{-/-}$ x rtTA x WT *DNMT3A* as previously described (Ketkar et al., 2020)) was transplanted into lethally irradiated C57Bl/6-CD45.1 recipients and allowed to engraft for 4 weeks. Engraftment was assessed as

outlined above. Fully engrafted recipients were then fed 10,000 ppm doxycycline chow (Gateway Lab Supply; St. Louis, MO) to induce *DNMT3A* transgene expression.

METHOD DETAILS

Collection and processing of whole bone marrow

Femur, tibia, and pelvis-derived bone marrow cells were collected from mice in RPMI media (Gibco) with 15% FBS (Atlanta Biologicals). Bone marrow and peripheral blood were treated with Ammonium Chloride/KCl (ACK) red cell lysis buffer and resuspended in the RPMI/FBS mixture as a working solution. Lethal irradiation was performed by exposing mice to two doses of 550 rads four hours apart. CD45.1 recipients were purchased from Charles River Laboratories.

Floxing efficiency assay

PCR was performed using a 40-cycle program of 20 s at 94°C, 20 s at 65°C, and 30 s at 72°C per cycle. For *Dnmt3a* amplification, F1 primer (5′-CGGTCATTCCAGATGATTCCTC-3′) and R1 primer (5′-TGCTGT GGATGT-AGGAAAGCTG-3′) were used. For *Actin* amplification F1 primer (5′-CGGGCTGTATTCCCCTC CATCG-3′) and R1 primer (5′-GCCATGTTCAATGGGGTACTTCAGGG-3′) were used. cDNAs were normalized with *Actin* copy numbers calculated based on quantitative PCR using SYBR green. Floxing efficiency in whole bone marrow was calculated using a standard curve where 100% floxing was defined as floxing in germline *Dnmt3a*$^{fl/fl}$ x (*CMV*-Cre) mice and 0% floxing was defined as floxing in *Dnmt3a*$^{fl/fl}$ x Cre negative samples.

Whole-genome bisulfite sequencing

WGBS was performed as described in Smith et al. (Smith et al., 2021), using the AccelNGS Methyl-Seq DNA library kit (Swift Biosciences, #30096). Sequence was generated on Illumina HiSeq or NovaSeq instruments and reads were mapped with biscuit (version 0.3.8), and DMRs were called using metilene (Juhling et al., 2016) as previously described (Cole et al., 2017; Spencer et al., 2017; Ketkar et al., 2020). The workflow for WGBS data is described in detail at https://github.com/genome/analysis-workflows/blob/master/definitions/pipelines/bisulfite.cwl (commit id: 174f3b2).

FACS sorting of cell populations

Bone marrow cells were isolated from femurs and tibias and treated with ACK red cell lysis buffer. Cells were stained with combinations of the following antibodies against cell-surface markers to identify indicated cell types (all antibodies are from Becton Dickinson unless indicated; clone indicated in parentheses): CD11b (MI/70), Gr1 (TB6-8C5; Biolegend), Ter-119 (Ter119), CD71 (C2), B220 (RA3-6B2), CD3e (145-2C11), Sca-1 (D7; Biolegend), c-KIT (2B8), CD34 (RAM34), FLT3 (A2F10; Biolegend), CD150 (TC15-12F12.2; Biolegend), CD48 (HM48-1; Biolegend), CD45.1 (A20), CD45.2 (104). Bone marrow and LinKit donor cells were isolated from transplanted mice using CD45.1-/CD45.2+ gating prior to selection for immunophenotypically defined populations. The following phenotypes were used to define stem and progenitor populations for sorting and Dnmt3a flow cytometry: Lineage (Lin): CD11b+, Gr1+, Ter119+, CD71^{+}, B220+, CD3e+; LSK: Lin-, Sca-1+, c-KIT+; GMP: Lin-, Sca-1+, c-KIT+, CD34^{+}, FLT3+; CMP: Lin-, Sca-1+, c-KIT+, CD34^{+}, FLT3-; MEP: Lin-, Sca-1+, c-KIT+, CD34-, FLT3-. Sorting was performed on a modified Sony Synergy SY3200 (Sony Biotechnology, San Jose, CA) updated to 24 parameters. Winlist version 8 software was used for data acquisition and analysis (Verity Software House, Topsham, ME).

Single cell RNA sequencing

Single-cell RNA libraries were created using the 10x Genomics Chromium Single Cell 5′ Kit and aligned with CellRanger (version 3.1). Using a nearest neighbor algorithm implemented in R (version 3.5.1), cells were annotated according to the Haemopedia expression atlas of hematopoietic cell types (de Graaf et al., 2016) using code available here at https://github.com/genome/docker-scrna_lineage_inference. The characteristics of each sample are summarized in (Ketkar et al., 2020). Using Partek Flow software build 10.0.21.0411, we eliminated the analysis of cells that contained fewer than 250 expressed genes, less than 500 total reads, or more than 10% mitochondrial transcripts. For each cell, expression of each gene was normalized to the sequencing depth of the cell, scaled to a constant depth (10,000), and log-transformed. Dimensionality reduction and visualization were performed with the t-SNE algorithm. Full details and parameters used are described in (Ketkar et al., 2020).

QUANTIFICATION AND STATISTICAL ANALYSIS

Quantification was performed as described in the relevant method details sections above. Statistics were performed as described above using metilene (v0.2.6), bsseq (v1.18.0) Partek flow software (build 10.0.21.0411), R (v4.1.0) and GraphPad Prism (v9.3.1). Standard statistical tests used are described in the results and figure legends.